Ore Geology Reviews 38 (2010) 101–112

Contents lists available at ScienceDirect

Ore Geology Reviews

journal homepage: www.elsevier.com/locate/oregeorev

Epithermal gold mineralization at Wadi Abu Khushayba, southwestern Jordan

M. Al-Hwaiti [a], B. Zoheir [b,*], B. Lehmann [c], I. Rabba [d]

[a] Department of Environmental Engineering, College of Mining and Environmental Engineering, Al-Hussein Bin Talal University, P.O. Box (20), Ma'an, Jordan
[b] Department of Geology, Faculty of Science, Benha University, 13518 Benha, Egypt
[c] Mineral Resources, Technical University of Clausthal, 38678 Clausthal-Zellerfeld, Germany
[d] Department of Exploration, Natural Resources Authority, Amman, Jordan

ARTICLE INFO

Article history:
Received 5 April 2010
Received in revised form 16 July 2010
Accepted 19 July 2010
Available online 24 July 2010

Keywords:
Epithermal gold
Shear zone
Wadi Abu Khushayba
Jordan

ABSTRACT

The Wadi Abu Khushayba area in southwestern Jordan hosts an auriferous, quartz-veined shear zone with features of an epithermal low-sulfidation gold system. The quartz-lode and quartz-carbonate mineralization is characterized by open-space textures, typically with sharp-walled veins and multi-stage brecciation of the late Neoproterozoic (~560 Ma) rhyolitic and granophyric host rocks. Silicic alteration by cryptocrystalline quartz is abundant; potassic alteration is expressed by muscovite and K-feldspar blastesis, commonly with dispersed hematite laths. Sulfide content is low. Relict pyrite and chalcopyrite occur in comb and cockade quartz. Gold occurs disseminated in the volcanic and subvolcanic wall rocks and as late vein infill.
The coexistence of vapor-rich and liquid-rich fluid inclusions in quartz, quartz textures, and the presence of adularia and calcite in the vein mineralogy suggest boiling concomitant with gold deposition in a structural setting favoring high fluid flow. Fluid inclusions in quartz define a temperature range of 350–380 °C and low salinity (~1.5–7 wt.% NaC1 equiv.) for the ore system. Pressure is estimated at 200–250 bars, indicating a maximum paleo-depth of 2500 m (hydrostatic). It appears likely that the Wadi Abu Khushayba system represents the near-surface epithermal expression of a larger unexposed mesothermal system. Such mesothermal systems are typical elsewhere in the Arabian–Nubian Shield, but are not exposed in southwestern Jordan where the present-day erosional level is close to the unconformity of the transgressive Early Cambrian platform sedimentation.

1. Introduction

The Panafrican Arabian–Nubian Shield in Arabia and northeast Africa consists largely of juvenile continental crust of Neoproterozoic age (Dixon and Golombek, 1988; Hargrove et al., 2006). This region formed mainly by accretion of volcanic island arcs in the time interval between ~870 and 550 Ma, and widespread systems of hydrothermal quartz veins attest to extensive fluid flow related to metamorphic dehydration and post-orogenic felsic magmatism (e.g., Almond et al., 1984; Loizenbauer and Neumayr, 1996; Tolessa and Pohl, 1999; Kusky and Ramadan, 2002). The quartz veins were the target of early gold mining, as shown by thousands of ancient workings, generally marked by excavations, tailings, slag piles, and village ruins, scattered throughout the Arabian–Nubian Shield (e.g., El Ramly et al., 1970; Sabet and Bondonosov, 1984; Gabra, 1986; Pohl, 1988; Sabir, 1991; Béziat et al., 1995).

Ancient mining in Jordan (3500 BC) was focused on the Early Cambrian sediment-hosted copper mineralization of the Faynan district (Fig. 1; Hauptmann, 2007). Recently, regional stream-sediment prospecting led to the discovery of gold anomalies in the Abu Khushayba area in the central part of Wadi Araba, ~250 km south of Amman and 110 km north of Aqaba (Bullen et al., 1996) (Fig. 1). This area is close to the Dead Sea depression, where the Neoproterozoic basement is exposed at a level close to the Cambrian erosional paleosurface. During the last decade, a detailed mapping and exploration programme by the Natural Resources Authority of Jordan led to the definition of a multiply brecciated linear NNW-trending zone in rhyolitic basement rocks. Gold contents reach up to 15 g/t in grab samples (Rabba et al., 1999; Abu Laila and Al-Saudi, 2002). However, mineralogical studies and an understanding of the ore system are lacking.

In the present study we report new structural, mineralogical, geochemical and fluid-inclusion data which document the Abu Khushayba gold prospect as a low-sulfidation epithermal system. The preservation of this relatively shallow system is unusual because large parts of the Arabian–Nubian Shield are deeply eroded, and most lode-gold deposits studied so far are of mesothermal style (e.g., LeAnderson et al., 1995; Harraz, 2000; Helmy et al., 2004; Zoheir, 2008).

2. Geological setting

The basement rocks exposed in southwestern Jordan are subdivided into the Aqaba and Araba complexes (Rashdan, 1988; Jarrar et al., 1991;

* Corresponding author.
E-mail address: basem.zoheir@gmail.com (B. Zoheir).

0169-1368/$ – see front matter
doi:10.1016/j.oregeorev.2010.07.002

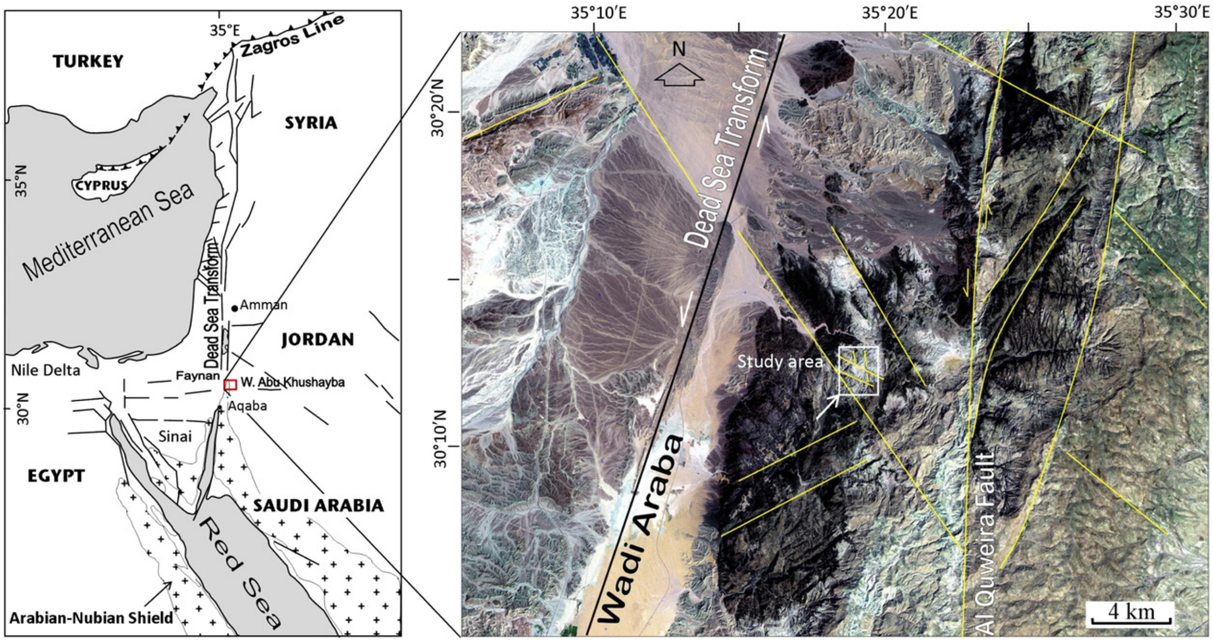

Fig. 1. Location map and ETM + (7-4-2) Landsat 7 image showing the fault pattern of the study area including the currently active Dead Sea Transform (solid black), offsetting Pleistocene–Recent alluvial fans along Wadi Araba (Garfunkel, 1981), and other older strike-slip faults inactive at present (e.g., the Al Quweira fault) and NW–SE faults. Normal NNW–SSE faults are considered as last reactivation along an older strike-slip fault trend.

Ibrahim and McCourt, 1995). The Aqaba (older) and Araba (younger) complexes comprise igneous and metamorphic suites, mostly of late Proterozoic age. These complexes are separated by a regional unconformity (peneplanation), which is represented by the Saramuj Conglomerate Formation. The Aqaba complex (800 to ~570 Ma) consists mainly of calc-alkaline plutonic igneous and metamorphic rocks, whereas the Araba complex comprises the Safi and Finan granitic suite, and Qirenifat and Ahaymir volcanic suites (Rabba and Ibrahim, 1988). The calc-alkaline granitic, andesitic and rhyolitic rocks exposed along the eastern escarpment of Wadi Araba in southwest Jordan, which represent a part of these Late Protozoic complexes (Rashdan, 1988), are unconformably overlain by Phanerozoic sedimentary rocks, which have been affected by young tectonics largely associated with the Dead Sea Transform fault system (Barjous, 1992).

The N–NE-trending Wadi Araba Fault is the most prominent structural feature in the study area (Fig. 1). This structure is manifested by the Wadi Araba depression (Jordan rift valley), straight scarps in Pleistocene and Recent sediments, sudden changes in the drainage courses, and a line of springs on the downthrown side of the Wadi Araba. The Al Quweira Fault, ~15 km east of the Araba Fault, is a ~N-trending fault extending for several hundreds of km from Saudi Arabia in the south to the Finan area in southern Jordan. Barjous and Mikbel (1990) suggested that the Al Quweira Fault accommodates a sinistral displacement of 40 km. According to several authors (e.g., Lenz et al., 1972; Bender, 1974; Barjous and Mikbel, 1990, and references therein), the Al Quweira Fault may represent an old zone of structural weakness, along which the Precambrian Ahaymir volcanic suite have been emplaced. The area between the Wadi Araba and Al Quweira faults is densely dissected by a set of parallel NW–SE antithetic step-faults south of Wadi Abu Khushayba (Fig. 1). The geomorphology of the study area is chiefly controlled by the geometric patterns of the NNE–SSW fault sets and by their intersection with the NW- to NNW-trending normal faults (cf. Bender, 1974).

2.1. Field description

The basement rocks exposed in the study area comprise granite, volcanic and volcaniclastic sequences and subordinate metasedimentary rocks (Fig. 2). The metasedimentary rocks are mainly metagraywacke and -siltstone forming an elongate slab along the tectonic contact (strike-slip fault) between granite and rhyolite in the southwestern part of the study area. The granitic rocks vary from monzogranite to syenogranite, characteristically with hypidiomorphic texture and equal amounts of biotite and muscovite, and K-feldspar dominates over oligoclase-andesine. In terms of field relationships and mineralogical composition, these rocks are similar to the Huwar two-mica granite suite which is common in southwestern Jordan (U–Pb zircon age of 569 ± 11 Ma: Jarrar et al., 1983). Feldspar and quartz-mica pegmatites occur in zones where the granitic rocks are densely dissected by cross-cutting faults.

The volcanic rocks exposed in the study area are part of the Ahaymir Volanic Suite of Bender (1974), which includes rhyolite flows (Qusayb Rhyolite), and lithic tuffs, breccias and agglomerates collectively known as Mussaymir Volcanic Effusives. The Qusayb Rhyolite occurs as reddish brown rocks with large albite and orthoclase phenocrysts in a microcrystalline quartz-feldspar groundmass. The boundaries of the Qusayb Rhyolite are mainly tectonic, and structural fabrics including fault striations and gouges suggest episodic reactivation along these contacts. Irregular and elongate enclaves of granite are common in the Qusayb Rhyolite near the contact with the granite body in the southwestern part of the study area. The Mussaymir Volcanic Effusives form a NW-trending belt in the central part of the study area. These rocks are dominated by xenolithic agglomerate, volcanic breccia, lithic tuff, rhyolitic tuff and quartz porphyry (Rabba, 1994). The xenolithic agglomerates occur as greenish rocks with cryptic bedding. Xenoliths are mainly granite, gneiss and schist. The felsic volcanic rocks, including quartz porphyry, rhyolitic tuff and volcanic breccias, yielded an age range of 540–550 Ma based on Rb–Sr isochrons (Brook and Ibrahim, 1987). The Mussaymir Volcanic Effusives include porphyritic rhyolitic flows, commonly associated with thin offshoots of fine-grained granite, and breccias with abundant granitic fragments (e.g., McCourt, 1988). The auriferous shear zone studied is developed in porphyritic rhyolitic flows of the Mussaymir Volcanic Effusives, especially where cut by offshoots of granophyre.

The Neoproterozoic sequence of igneous rocks is unconformably overlain by a flat-lying Early Paleozoic sedimentary cover

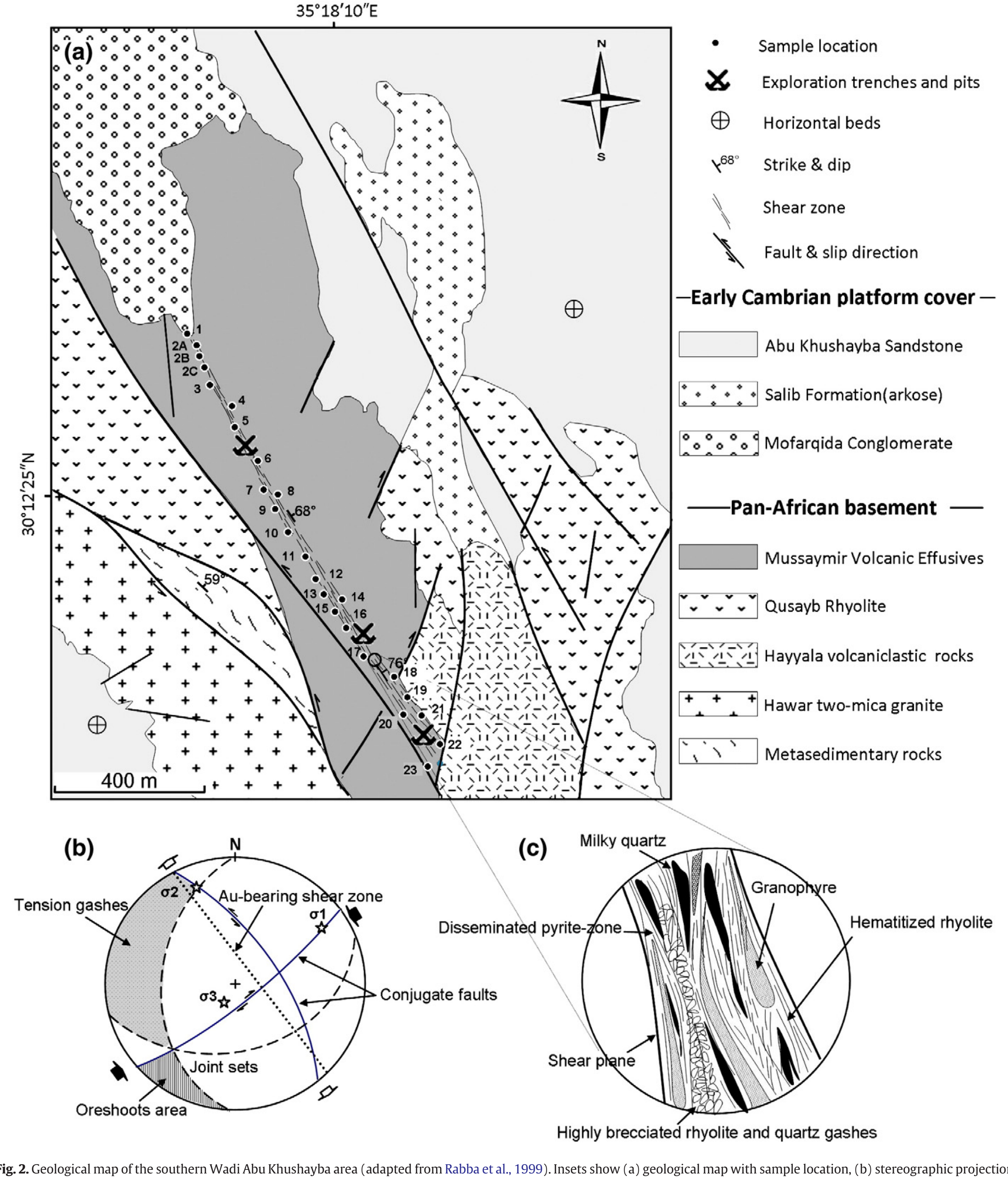

Fig. 2. Geological map of the southern Wadi Abu Khushayba area (adapted from Rabba et al., 1999). Insets show (a) geological map with sample location, (b) stereographic projection of the fault/joint and shear planes and stress component directions, and (c) details of the internal structure of gold-quartz veined shear zone.

sequence. The basal Mofarqida Conglomerate consists of polymictic, angular to subrounded, poorly-sorted cobbles and boulders of the basement rocks, overlain by sandstone. The Early to Late Cambrian Salib Formation and Abu Khushayba Sandstone consist of coarse- to fine-grained micaceous sandstone to siltstone with fragments of volcanic basement rocks. These rocks represent a spectrum of continental alluvial to shallow marine clastic sedimentation, and host important stratabound copper mineralization (Rabba et al., 1999; Hauptmann, 2007).

The study area is dissected by numerous faults trending mainly in two major directions, NW–SE and NNE–SSW. Based on field observations and interpretation of satellite data interpretation, these trends represent a system of conjugate faults developed under a compressional stress regime in which σ_1 was oriented NE–SW and σ_3 was perpendicular to the paleosurface (see Fig. 2). Subsequently, during later stages of evolution and uplift, the stress direction rotated by 90° so that σ_1 was perpendicular to the surface instead of σ_3. This system of conjugate faults is best developed in the basement rocks, and is missing or rarely reactivated in the Cambrian and younger sedimentary rocks. This observation suggests a pre-Cambrian age of the fault system and associated fabrics.

A narrow shear zone, dipping steeply to the NE and cutting through the Mussaymir Volcanic Effusives, is associated with quartz lenses and gashes, and brecciated wallrocks converted to hematite-sericite rock, in the central part of the study area (Fig. 3). It extends for approximately 1 km m in a NNW–SSE direction and varies in thickness from 0.4 to 1.5 m. This shear zone is composed of variably deformed, intermixed hematite-coated microcrystalline quartz and quartz-rich rhyolitic breccia and lithic tuffs with or without subordinate amounts of hydrothermal carbonate. Domains with disseminations of pyrite, partially or completely altered to goethite, exhibit a pale to deep greenish or brownish color.

A volcanic breccia with variable contents of angular rhyolite fragments has been observed in zones of dense intersections of fault and joint sets. Disseminated carbonate (calcite) is common in the interstitial spaces of brecciated rocks within and adjacent to the mineralized shear zone. Hematite occurs as disseminations or veinlets interstitial in the fine-grained matrix or along microcracks. Rhyolitic breccia and lithic tuffs contain pyrite disseminations in the fine-grained matrix. The hematite-coated quartz-rich breccia is made up mainly of different types of fragments including granite, schist, granophyre, andesite and dacite. These components are cemented by microcrystalline quartz and minor carbonate. Accessory minerals comprise rutile and magnetite. Narrow offshoots of granophyre (<15 cm wide) consist essentially of quartz, K-feldspar and less common andesine-albite.

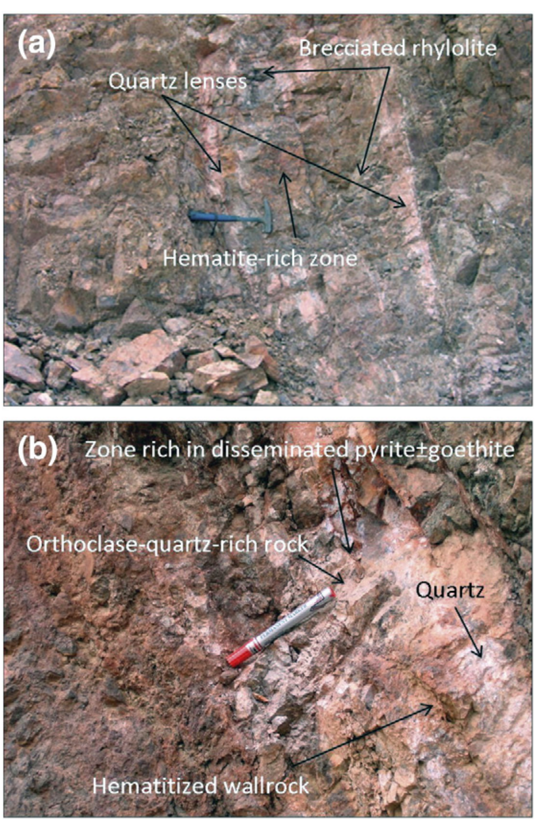

Fig. 3. Features of the mineralized shear zone showing internal structures: (a) intermixed quartz, brecciated ryholite and microcrystalline quartz-rich rock; and (b) quartz veining in pervasively hematitized granopyhre/rhyolite.

3. Analytical methods

Major- and trace-element analyses of the host volcanic rocks were done by X-ray fluorescence spectrometry at the Federal Institute for Geosciences and Natural Resources (BGR), Hannover, Germany. Concentrations of major elements were determined using pellets of rock powder mixed with $Li_2B_4O_7$ (1:9) and fused at 1120 °C, whereas trace-element analyses were performed on pressed powder pellets. Analytical precision estimated from duplicate analyses is better than 3% for major elements and between 5 and 10% for trace elements. Gold and silver contents in selected samples have been determined using the simultaneous multi-element neutron activation and ICP-AES (total digestion) techniques at the BGR.

The chemical composition of some ore minerals was measured using a CAMECA SX-100 electron microprobe equipped with four wavelength-dispersive spectrometers and a Noran energy-dispersive spectrometer at the Technical University of Clausthal. The applied standard operating conditions for most elements were 30 kV accelerating potential and 40 nA beam current, with analysis for Au, Ag and Ni at 300 nA beam current. Count times ranged from 10 to 400 s. Standards used were pure elements and oxides.

Microthermometric measurements were carried out on ~150 µm-thick doubly-polished wafers using a Linkam THMSG-600 heating/freezing stage at the fluid-inclusion laboratory of the Mineral Resources group, Technical University of Clausthal. Measurements were carried out following the procedures outlined by Shepherd et al. (1985). The accuracy of the microthermometric results has been checked by regular calibration using inorganic melting-point standards and synthetic fluid inclusions. A heating rate of 1 °C/min was used to record phase changes below 30 °C, whereas a heating rate of 5 °C/min was used for phase changes above this temperature. Hence, low-temperature phase changes are accurate to ±0.2 °C, whereas temperatures above 30 °C have an estimated accuracy of ±2 °C.

4. Host-rock geochemistry

Twenty-five representative samples of volcanic and subvolcanic (granophyre) rocks hosting the auriferous shear zone were chosen for a geochemical study in order to depict petrochemical characteristics and tectonic setting. The data obtained (Table 1) indicate a generally felsic composition with high silica contents (65.9–87.6 wt.% SiO_2) and variable alumina and alkali contents (4.9–12.9 wt.% Al_2O_3, 3.7–10.3 wt.% K_2O, 0.1–2.5 wt.% Na_2O). These compositions are variably affected by silicic and potassic alterations. Most samples plot in the rhyodacite/dacite field on the immobile-element classification diagram of Winchester and Floyd (1977) (Fig. 4a). The tectonomagmatic discrimination diagram of Pearce et al. (1984), using the relatively immobile elements Nb and Y, indicates that the investigated volcanic rocks developed in a volcanic-arc environment (Fig. 4b).

Multi-element neutron activation and ICP (total digestion) analyses on the samples from the mineralized quartz veined wallrocks and host rocks with disseminated ores indicate the presence of Au and Ag contents ranging from traces up to 35 g/t Au and 108 g/t Ag, respectively (Table 2). Means and standard deviations for intensively silicified (quartz-veined) samples are 12.7±9.1 g/t Au and 35±27 g/t Ag (n=16), respectively, whereas the non-veined wallrock samples with disseminated ore (n=9) have 0.24±0.15 g/t Au and 3.07±2 g/t Ag, respectively, signifying quartz-veining as an important process in ore formation at the study area. The data reveal that Au show weak positive correlation with few elements including Ag, Cu and Ba (R^2=0.46, 0.13 and 0.10 respectively) but shows no correlation with any other elements. This lack of correlation is likely due to processes of supergene redistribution where Au and Ag would be less mobile than other ore components. The common pathfinder elements arsenic and antimony are only slightly enriched over bulk continental crust (Taylor

Table 1
Representative major (wt.%) and trace element (ppm) data of volcanic (volc.) and granophyric (subvol.) rocks from Wadi Abu Khushayba area.

Sample	K-1	K-2A	K-2B	K-2C	K-3	K-4	K-5	K-6	K-7	K-8	K-9	K-10	K-11	K-12	K-13	K-14	K-15	K-16	K-17	K-18	K-19	K-20	K-21	K-22	K-23
Description	Volc.	Subvol.	Subvol.	Subvol.	Volc.	Volc.	Volc.	Volc.	Volc.	Volc.	Volc.	Volc.	Volc.	Volc.	Volc.	Subvol.	Subvol.	Volc.	Volc.	Volc.	Subvol.	Volc.	Volc.	Volc.	Volc.
SiO_2	75.32	87.59	80.46	86.20	72.89	72.80	77.61	76.24	72.29	76.50	78.60	79.47	78.92	79.45	79.68	86.01	81.85	78.10	77.96	78.55	83.20	65.93	66.87	78.57	74.29
Al_2O_3	11.51	4.99	8.39	6.03	12.55	12.43	9.76	11.65	11.68	11.35	8.92	9.22	10.11	9.00	9.01	5.61	7.98	8.44	10.78	10.20	7.55	12.39	12.91	8.33	10.06
Fe_2O_3	1.81	1.80	2.08	2.09	1.04	2.29	2.69	1.48	4.69	1.25	2.06	2.78	1.49	2.84	2.64	2.94	2.54	1.36	0.99	1.88	1.83	8.05	6.37	2.95	3.80
MgO	0.24	0.25	0.20	0.23	0.26	0.43	0.56	0.07	1.02	0.16	0.20	0.56	0.15	0.38	0.51	0.27	0.32	0.23	0.04	0.18	0.08	0.10	0.50	0.60	0.49
CaO	0.51	0.49	0.82	0.20	0.48	0.56	0.41	0.13	0.54	0.24	1.17	0.30	0.17	0.26	0.26	0.12	0.22	2.35	0.32	0.17	0.30	0.92	0.89	1.29	1.47
Na_2O	0.18	0.10	0.20	0.50	0.18	0.61	0.23	0.16	2.50	0.15	0.23	1.22	0.31	0.38	0.69	0.17	0.41	0.26	0.16	0.19	0.10	0.19	0.71	0.21	1.20
K_2O	9.17	3.74	6.54	3.78	10.33	9.14	7.24	9.73	4.75	9.41	7.16	5.00	8.05	6.39	5.82	4.02	5.72	6.52	9.06	8.01	6.19	10.34	8.93	5.85	4.01
TiO_2	0.07	0.05	0.06	0.10	0.01	0.11	0.20	0.03	0.45	0.03	0.08	0.20	0.05	0.13	0.14	0.06	0.11	0.06	0.03	0.08	0.04	0.49	0.45	0.25	0.52
P_2O_5	0.03	0.03	0.03	0.04	0.02	0.05	0.07	0.02	0.16	0.03	0.04	0.07	0.03	0.04	0.05	0.03	0.04	0.03	0.03	0.04	0.03	0.12	0.08	0.12	0.20
MnO	0.14	0.13	0.14	0.16	0.09	0.13	0.16	0.13	0.15	0.12	0.20	0.16	0.17	0.15	0.16	0.14	0.16	0.12	0.09	0.13	0.16	0.18	0.10	0.17	0.17
LOI	0.78	0.60	0.83	0.52	0.62	1.06	0.82	0.15	1.45	0.47	0.99	0.83	0.31	0.76	0.81	0.50	0.49	2.19	0.32	0.34	0.33	0.83	1.80	1.11	2.92
Σ	99.76	99.77	99.75	99.84	98.47	99.61	99.74	99.79	99.68	99.70	99.65	99.81	99.76	99.78	99.78	99.88	99.83	99.66	99.77	99.76	99.80	99.53	99.61	99.44	99.12
Ba	802	401	619	315	8229	1187	669	706	1008	585	777	520	803	621	803	417	596	1097	1005	843	593	1951	1209	2398	3694
Rb	320	129	231	129	363	315	248	320	141	320	219	177	271	219	192	131	166	187	293	240	191	239	317	198	96
Sr	72	42	71	46	146	105	80	85	80	93	68	80	74	59	66	44	46	69	82	80	55	44	59	92	136
Nb	3	–	–	3	–	–	6	–	9	–	3	5	4	7	4	3	3	5	–	3	–	27	31	6	9
Th	11	11	9	13	8	10	12	10	18	10	10	15	10	14	12	10	10	11	8	11	12	18	19	14	18
Y	6	5	4	5	4	8	13	4	24	6	8	10	6	10	9	6	6	6	7	8	4	40	43	12	19
Zr	33	21	26	42	10	46	86	13	177	16	39	90	27	87	67	33	50	26	16	32	19	335	421	90	188
Ce	–	8	6	10	4	8	24	8	43	8	11	16	4	16	13	6	25	5	8	8	4	64	71	21	40
Ga	9	4	6	6	6	10	10	6	16	7	7	9	6	11	10	6	7	5	5	7	5	10	24	9	16
La	3.7	4.7	4.4	6.4	2.7	4.6	15.3	3.8	25.1	5.0	8.8	7.6	3.1	8.3	7.4	2.5	26	2.3	6.3	4.9	3.5	36.2	45.0	11.9	22.0
Lu	–	–	0.08	0.08	–	0.06	0.13	–	0.30	0.06	0.08	0.20	–	0.19	0.13	0.07	0.11	–	–	–	–	0.69	0.89	0.18	0.38

(–) Below detection limit.

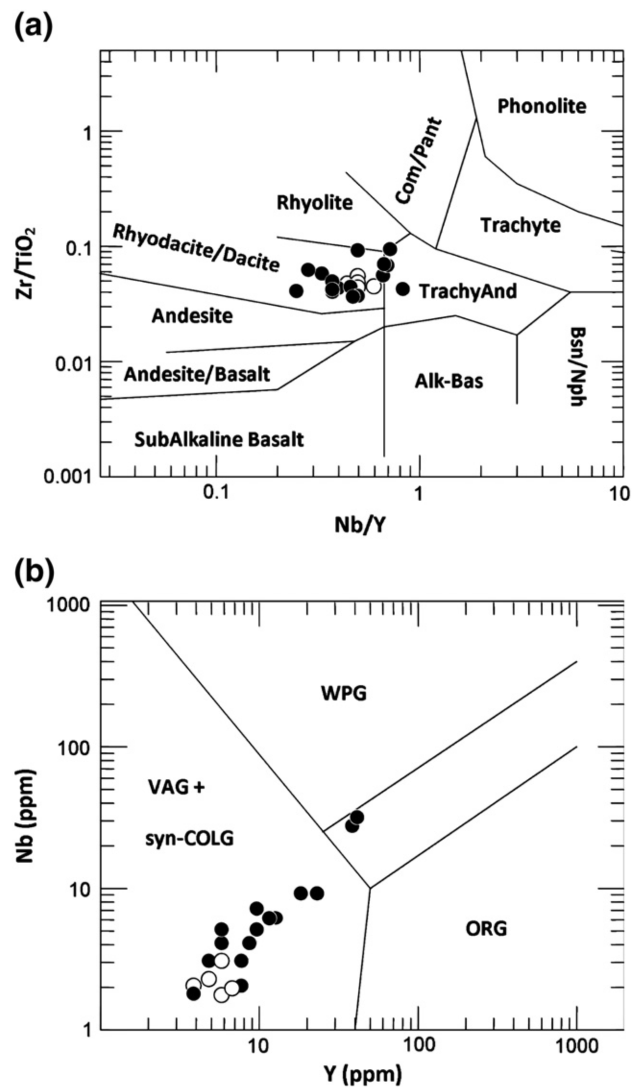

Fig. 4. Geochemical characteristics of the volcanic and sub-volcanic (granophyric) host rocks. (a) Zr/TiO_2 *vs.* Nb/Y classification diagram of Winchester and Floyd (1977). (b) Nb *vs.* Y discrimination diagram of Pearce et al. (1984). Solid dots represent the volcanic/volcaniclastic rocks; open circles represent the granophyric (sub-volcanic) rocks. VAG = volcanic arc granites, syn-COLG = syn-collsion granites, WPG = within-plate granite, ORG: ocean ridge granite.

and McLennan, 1995), i.e., 4.6 ± 3.2 ppm As and 1.4 ± 0.6 ppm Sb (n = 25), which may be due to superficial leaching.

5. Gold mineralization

Gold mineralization is related to the NNW-trending shear zone and associated quartz lenses and gashes in the central part of the study area. This shear zone comprises fragments of brecciated rhyolitic tuff, xenolithic agglomerates and tectonized granophyric bands (Fig. 5a–c). Bleached and silicified wallrocks form a ~10 m wide zone with quartz and Fe–Mn oxide-rich veinlets with significant Au contents. Evidence of both ductile and brittle deformation is observed, i.e., subgrain development and bulging recrystallization along some microshears, and mortar textures in large crystals of quartz (Fig. 5d, e). Shearing along the newly developed brittle planes led to formation of dilation sites, in which comb quartz developed together with disseminated aggregates of gold. Drusy, feathery, banded, and cockade quartz textures together with pyrite aggregates are common in vugs and open spaces, likely developed later in the history of the shear zone. Comb structure, consisting of parallel quartz crystals oriented perpendicular to the vein walls, is common in the significantly mineralized samples (Fig. 5e). Crustiform and colloform quartz textures are absent. In addition to quartz, some bands contain subordinate adularia of rhombic shape (Fig. 5f), carbonate, sulfides (particularly pyrite and chalcopyrite) and kaolinite. Quartz and sulfide minerals commonly form cockade overgrowths around the brecciated fragments.

Within and alongside the mineralized shear-zone, destruction of the wallrock textures and primary minerals is incomplete, so that their original characteristics are still recognizable. Plagioclase (andesine and albite) microphenocrysts are altered to white mica with finely crystalline quartz. The white mica is disseminated in the matrix of the volcanic rocks and fills open spaces. Propylitic alteration, which represents the outermost hydrothermal alteration halo, occurs around the veins and quartz-white mica zones. It forms a diffuse halo where the original texture of the host rocks has been preserved, and is mainly restricted to phenocryst phases. Biotite flakes are partially or completely chloritized. Quartz filling the open spaces exhibits variable textures, including massive milky quartz alternating with transparent bands, in which fine-grained quartz and chalcedony occur as successive, narrow bands with alternating pale colors in exposure. Recrystallization textures include plumose quartz crystals with feathered or splintery extinction, mosaics of microcrystalline quartz, and interpenetrating grain-boundaries. Barite occurs as ~0.3 cm across, relatively clear crystals, forming a network of veinlets less than 1 cm in width, cutting the quartz veins. "Adularia" (K-feldspar) is an occasional component in the mineralized veins, forming subhedral to euhedral cuneiform crystals with rhombic sections (Fig. 5f).

The ore mineralogy of the shear zone is relatively simple, indicating a single stage of mineralization. Ore minerals include pyrite and chalopyrite, partially or completely altered to rhythmic goethite and abundant disseminated hematite (Fig. 6a–d). Gold occurs as micrometric blebs, globules and specks disseminated along microfractures in quartz or associated with altered pyrite (Fig. 6e, f). A paragenetic link between gold and pyrite is suggested on the basis of the close spatial association between gold and altered pyrite. The occurrence of gold only in association with altered sulfides may suggest that gold was refractory in pyrite and/or chalcopyrite, and was liberated and redistributed by late alteration.

Table 2
Gold and other trace element contents (ppm) in volcanic and subvolcanic rocks from Wadi Abu Khushayba area.

Sample	Det. limit (ppm)	Method[a]	KH-1	KH-2A	KH-2B	KH-2C	KH-3	KH-4	KH-5	KH-6	KH-7	KH-8	KH-9	KH-10
Au	0.002	INAA	30	1.14	3.84	0.756	15.8	7.7	0.742	1.69	0.665	2.78	0.313	11.1
Ag	0.3	MULT INAA / TD-ICP	108	68.9	78.2	6.1	19.4	19.9	15.3	15	0.7	3.2	11.3	15.3
Cu	1	TD-ICP	122	164	124	143	659	380	246	27	22	236	82	73
Pb	3	TD-ICP	17	13	12	14	88	38	81	9	122	34	18	17
Zn	1	MULT INAA / TD-ICP	27	23	20	20	43	41	59	20	306	148	19	41
As	0.5	INAA	3.2	2.3	3.6	5.2	2	5.6	4	3.1	10	5.8	4.7	4.1
Cr	2	INAA	2	46	36	32	39	31	27	28	29	30	29	28
Mn	1	TD-ICP	1070	1060	979	1250	667	850	1130	838	1040	749	1410	1250

[a] Analytical methods: Multi-element INAA (Instrumental Neutron Activation Analysis) and TD-ICP (Total digestion-Inductively Coupled Plasma).

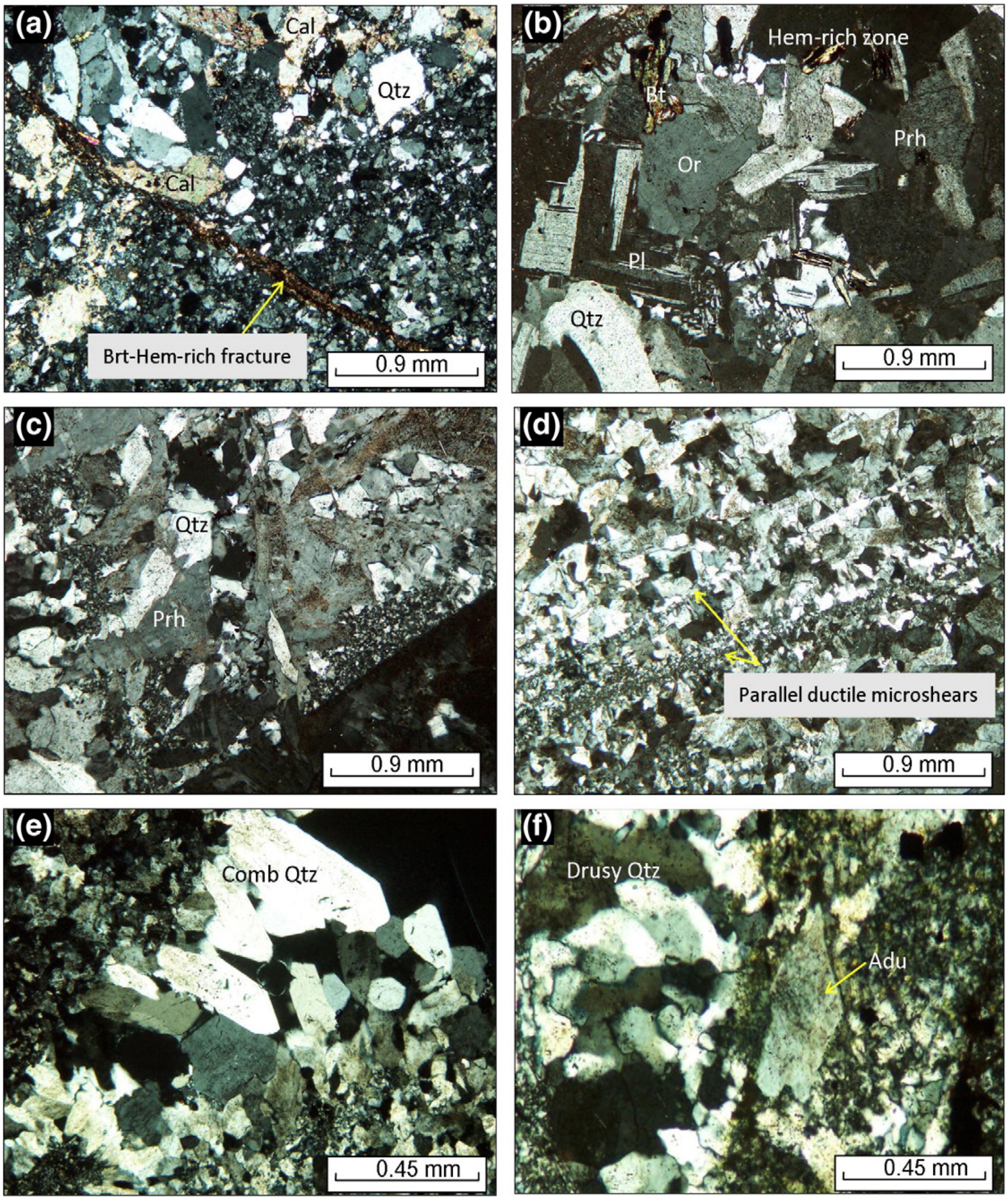

Fig. 5. Transmitted light photomicrographs illustrating microscopic features of the mineralized shear zone: (a) fine-brecciated rhyolitic tuff with disseminated calcite and pyrite next to microcracks filled with Fe-oxides; (b) K-feldspar rich granophyric band with abundant disseminated hematite; (c) tectonized granophyric band mainly of K-feldspar and quartz; (d) parallel shear planes and related subgrains and little brecciation indicating deformation under ductile conditions; (e) comb quartz filling spaces induced by non-coaxial simple shearing; and (f) drusy quartz associated with adularia in pervasively silicified wallrock within the shear zone. Abbreviations: Adu = adularia, Brt = barite, Bt = biotite, Cal = calcite, Hem = hematite, Kfs = K-feldspar, Pl = plagioclase, Prh = perthite, Qtz = quartz.

KH-11	KH-12	KH-13	KH-14	KH-15	KH-16	KH-17	KH-18	KH-19	KH-20	KH-21	KH-22	KH-23
0.403	0.268	0.426	0.121	0.888	0.157	0.912	0.618	0.12	0.163	0.075	0.789	0.158
2.8	1.1	5.4	0.4	1.7	0.3	1	1.3	3.3	0.8	1	0.9	0.7
77	26	107	15	38	248	52	16	26	14	11	33	371
11	22	37	22	16	27	9	23	17	51	70	8	28
15	46	49	26	34	30	16	27	15	17	140	29	31
4.6	2.4	3.5	4.1	3.4	2	1.9	2.3	2.5	6.8	5.8	4.3	16.9
22	23	29	25	25	19	23	19	28	28	12	28	24
1050	560	720	340	590	960	1080	780	510	1680	1220	2110	3880

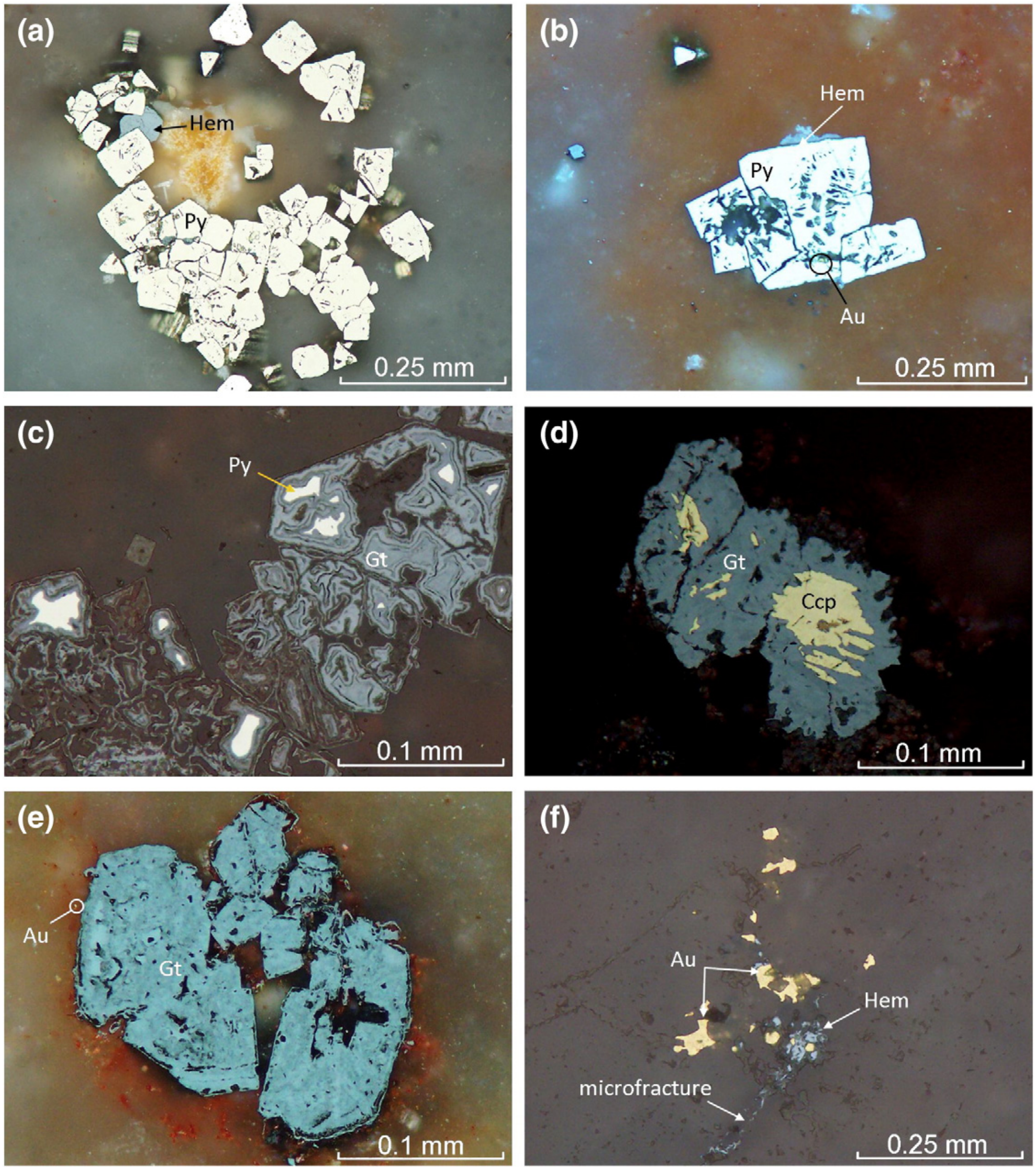

Fig. 6. Reflected light photomicrographs showing ore textures of the mineralized shear zone: (a) aggregated pyrite and hematite in rhyolitic breccia; (b) twinned pyrite crystals, replaced partly by hematite, with gold inclusion; (c) and (d) rhythmic goethite replacing more or less completely pyrite and chalcopyrite; (e) finely-dispersed gold specks occur at the totally altered sulfide crystal boundaries; and (f) remobilized gold and hematite along microfractures. Au—native gold, Cpy—chalcopyrite, Gt—goethite, Hem—hematite, Py—pyrite.

Electron-microprobe analyses (Table 3) revealed the presence of up to ~1 wt.% As in pyrite, and up to70 ppm Au and 80 ppm Ag. No correlation exists between As content in pyrite and Au or Ag content. It is also worthy that 70 or 80 ppm value is approaching the detection limit of the electron probe under the applied conditions (50 ppm for Au and Ag). Chalcopyrite, on the other side, showed considerable values of Au (up to 470 ppm), which can be reasonable. These data suggest that chalcopyrite was a potential host for refractory Au, which was released upon oxidation and hydrolysis. The gold aggregates have a high fineness (Au ≥ 95%) as is typical of supergene gold.

6. Fluid inclusions in gold-bearing quartz lodes

Fluid-inclusion petrography was done on several polished thick sections of the gold-bearing quartz lenses, from which three samples were chosen for microthermometric measurements. The presence of vein-growth microstructures, large unstrained crystals of quartz and weak deformation and recrystallization were the criteria used for sample selection.

6.1. Fluid inclusion types, mode of occurrence and microthermometry

The investigated gold-bearing samples of lode quartz are generally rich in trail-bound, clustered and isolated aqueous (H_2O–NaCl) inclusions. These inclusions vary in shape from negative crystal, elongate, rounded to irregular, with diameters typically from ~5 to 20 μm. They are generally two-phase inclusions at room temperature, with a liquid aqueous phase and a H_2O vapor phase of variable proportions (~20–80% of total inclusion volume), and lack any daughter mineral. No evidence was observed for either CO_2 or clathrate formation on heating runs after supercooling to −100 °C. Secondary aqueous inclusion populations in healed fracture planes are abundant. These inclusions exhibit an irregular to subspherical or elliptical shape, and are of highly variable size, up to ~30 μm. Some of

Table 3
Representative data set of the electron microprobe analyses of the ore minerals of the Abu Khushayba gold mineralization.

Pyrite	Wt.%														
Fe	45.97	45.82	45.78	45.75	46.01	45.23	46.03	45.67	45.96	45.57	45.86	46.03	45.35	45.74	45.76
S	53.43	53.14	53.21	53.33	53.47	53.27	53.61	52.81	53.34	52.84	53.04	53.00	52.61	52.94	52.91
Cu	–	–	–	0.12	0.13	0.14	–	–	–	0.21	–	–	0.65	–	–
Zn	–	–	–	–	–	–	–	–	–	–	–	–	–	–	–
As	0.52	0.47	0.46	0.42	0.69	0.41	0.62	0.23	0.11	0.44	0.37	0.64	0.96	0.11	0.14
Ag	–	–	–	–	0.08	–	–	0.07	–	–	–	–	–	–	–
Ni	–	–	–	–	–	–	–	–	–	–	–	–	–	–	–
Au	–	–	–	0.06	0.07	–	–	0.07	–	–	–	–	–	–	–
Te	–	–	–	–	–	–	–	–	–	–	–	–	–	–	–
Sum	99.92	99.43	99.45	99.68	100.5	99.05	100.3	98.85	99.41	99.06	99.27	99.67	99.57	98.79	98.81
Chalcopyrite wt.%									Gold wt.%						
Fe	32.80	32.80	32.43	32.06	31.7	32.6	32.11	30.95	–	–	–	–	–	–	–
S	33.69	34.17	34.80	33.43	34.51	33.25	34.09	34.27	–	–	–	–	–	–	–
As	–	–	–	0.11	0.43	0.51	0.34	–	–	–	–	–	–	–	–
Ni	–	–	–	0.12	0.42	-	0.29	0.32	–	–	–	–	–	–	-
Cu	32.52	31.94	31.57	33.20	32.06	33.19	33.07	33.81	–	–	–	–	–	–	–
Zn	0.01	0.04	0.67	0.30	0.03	0.05	0.03	0.03	–	–	–	–	–	–	–
Ag	0.08	0.12	0.07	–	0.06	–	–	0.05	2.78	2.60	1.72	2.04	1.97	1.40	2.88
Te	–	0.14	0.11	–	–	–	–	–	0.13	0.12	–	0.12	–	–	–
Au	–	0.47	–	0.36	–	0.25	–	0.23	96.15	95.38	97.78	97.58	97.37	97.73	96.26
Sum	99.1	99.68	99.65	99.58	99.21	99.85	99.93	99.66	99.00	98.03	99.59	99.71	99.34	99.12	99.14

(–) Below detection limit.
Detection limit for Au = 50 ppm, Ag = 50 ppm, and Te = 100 ppm.

these inclusions contain one-phase, liquid-filled inclusions, and others show highly variable liquid-to-vapor ratios within an individual healed microfracture. This variation may imply a necking-down process due to grain-boundary migration (Dubessy, 1994). Occasional measurements on these inclusions indicate their dilute (pure H_2O) composition. Accordingly, these inclusions were excluded from further measurements and interpretations based on their secondary genesis (unrelated to the gold mineralization event).

Microthermometric data were collected from inclusions in the less deformed quartz. The data obtained, including the temperature of total homogenization ($T_{h\ total}$) and of final melting of ice ($T_{m\ ice}$), are summarized in histograms (Fig. 7). The thermometric data were interpreted in terms of composition and density of the trapped fluids. Molar volumes, compositions and densities were calculated using the 'BULK' and 'ISOC' software packages (Bakker, 2003). Salinities from ice melting were obtained using the equation given by Bodnar (1993). Isochores were calculated applying the equation of state of Zhang and Frantz (1987). Total homogenization occurred into the liquid and less frequently into the vapor phase. $T_{h\ total}$ varies from 347 to 378 °C for inclusions homogenized into the liquid, and 351 to 397 °C for inclusions homogenized into the vapor phase (Fig. 8). In some cases, homogenization temperatures of the vapor-rich inclusions were not determined owing to the difficulty in visual estimations of homogenization to the vapor phase (e.g., Bodnar et al., 1985). In some other cases, a gradual fading of the meniscus was observed during the heating runs. Temperatures of ice melting ($T_{m\ ice}$) range between −4.8 and −0.9 °C and correspond to a salinity range of 1.6–7.6 wt.% NaCl equiv. (Bodnar, 1993). The bulk molar volumes of the measured inclusions range between 27.5 and 39.4 cm^3/mol. Bulk densities vary from 0.08 to 0.69 g/cm^3. Salinities are higher in inclusions homogenized to liquid than in those that homogenized to vapor.

6.2. Interpretation of the fluid-inclusion data

Fluid inclusions trapped under conditions of boiling or immiscibility are valuable *P–T* indicators because the homogenization temperature equals the formation temperature (Roedder and Bodnar, 1980), eliminating the need for a pressure correction to obtain the trapping temperature. The two populations of fluid inclusions (liquid-rich and vapor-rich) observed in the Abu Khushayba system homogenize to liquid and vapor, respectively, within a narrow temperature range suggesting entrapment under boiling conditions. The variations in homogenization temperatures in both populations are likely due to imperfect entrapment of the vapor-only and liquid-only phase, i.e., contributions of vapor in the liquid-rich inclusions, and of liquid in the vapor-rich inclusions during entrapment.

The salinity of the liquid-rich fluid inclusions varies from 3–7 wt.% NaCl equiv., and we assume a mean salinity of 5 wt.% NaCl equiv. for the location of the boiling curve in *P–T* space (Fig. 9). The intersection of the isochores for the liquid-rich inclusions (density = 0.42–0.69 g/cm^3) and for the vapor-rich inclusions (density = 0.08–0.21 g/cm^3) with the water–5-wt.% NaCl boiling curve defines a pressure of 200–250 bars at ~350–380 °C, which corresponds to the conditions of fluid entrapment. This low pressure identifies a shallow environment where hydrostatic conditions are likely. The 200–250 bar pressure then translates into a maximum depth of formation of the fluid system at about 2500 m.

7. Discussion

In the evolution of the Arabian–Nubian Shield, subduction processes terminated with the emplacement of calc-alkaline, collisional, I-type granitoids (670–610 Ma: Fleck et al., 1980; Stern and Hedge, 1985; Ibrahim and McCourt, 1995). Subsequently, a transition to an extensional tectonic regime occurred (Moghazi, 2003). In Egypt, rock units diagnostic for such an extensional tectonic regime are the 610–550 Ma Dokhan Volcanics and molasse-type Hammamat Sediments, which were intruded by post-orogenic A-type granites (Sylvester, 1989). Equivalent rock units in the northern part of the Arabian Shield include the Shammar Group (600–555 Ma), which consists of undeformed post-orogenic volcanic rocks interbedded with coarse continental clastic rocks (Baubron et al., 1976). In Jordan, the 595 Ma Hayyala volcaniclastic rocks and the Saramuj Conglomerate (Jarrar et al., 1993) are post-orogenic and have a composition similar to the Dokhan Volcanics and the Hammamat Group in Egypt. Moghazi (2003) suggested that the late Neoproterozoic post-orogenic extensional-related volcanic rocks are coeval with the formation of clastic basins at about 600 Ma all over the Arabian–Nubian Shield.

The Ahaymir Volcanic Suite, which hosts the Abu Khushayba gold mineralization, is comparable to the post-Hammamat felsites in the

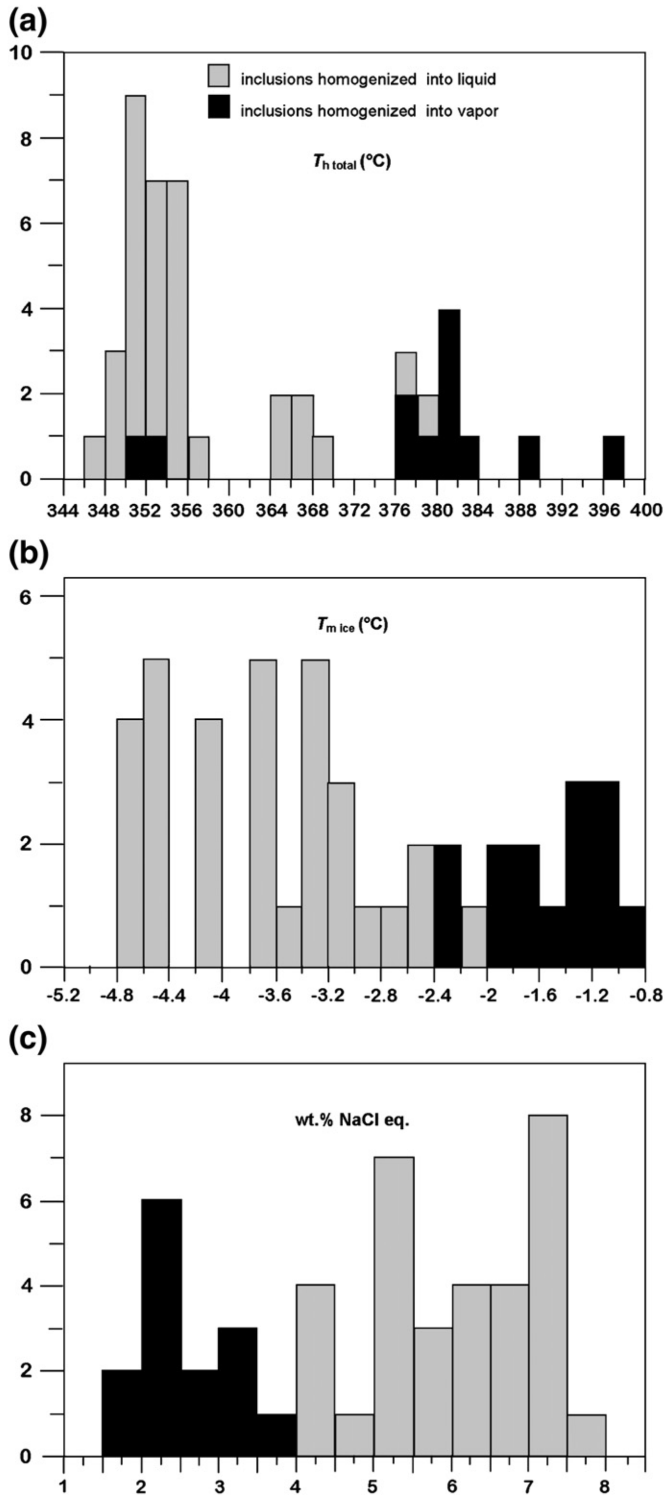

Fig. 7. Histograms of microthermometric data and salinities of fluid inclusions in auriferous quartz from the Abu Khushayba area.

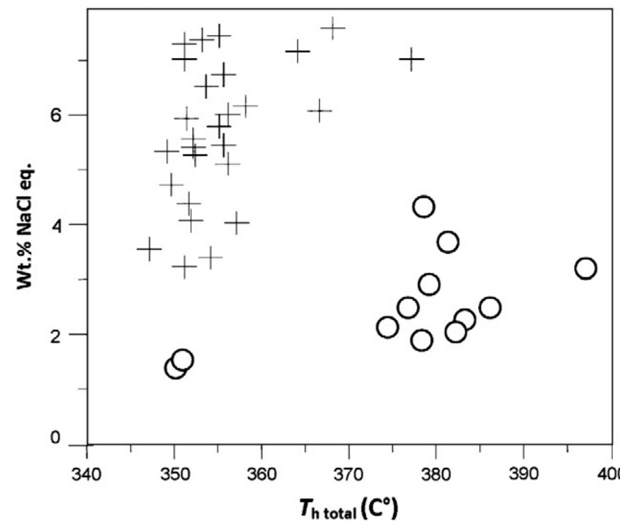

Fig. 8. Salinity *vs.* total homogenization diagram of the measured inclusions. Crosses represent fluid inclusions homogenized into liquid; open circles represent fluid inclusions homogenized into the vapor phase.

Egyptian part of the Arabian–Nubian Shield (Akaad and Noweir, 1969). Successions of rocks belonging or equivalent to this unit are widespread in the Sinai and in the northern parts of the Arabian Shield. These rocks are related to the Pan-African molasse stage (610–520 Ma: e.g., Baubron et al., 1976; Greenwood et al., 1976; Bielski, 1982; McCourt, 1988), and are known to host several gold deposits in the central and northern parts of the Eastern Desert (e.g., Atalla, Um Balad and Um Mongul). These deposits and other widespread Cu–Au mineralizations are suggested to have derived from an epithermal origin at relatively shallow depths (e.g., Garson and Shalaby, 1976; Hussein, 1990). It is, therefore, likely to propose a spatial/temporal relationship between gold mineralization and the Hayyala volcaniclastic rocks and related Ahaymir Volcanics, particularly in structural settings favoring fluid flow.

The auriferous quartz veins of the Arabian–Nubian Shield are closely associated with greenschist-facies rocks and generally confined to highly sheared granitoid and volcano-sedimentary rocks (Vail, 1987; Pohl, 1988). Most of these veins were formed under mesothermal (orogenic) conditions (e.g., Harraz, 2000; Doebrich et al., 2004; Zoheir, 2008). Less commonly, epithermal mineralization occurs in discrete parts of the Arabian Shield, commonly associated with (sub-aerial) volcanic rocks that form the upper part of subduction-related sub-volcanic potassic intrusives (e.g., Bakheit, 1991; Johnson et al., 2003). Two major gold deposits in the Arabian Shield, namely: Al Amar and Mahd adh Dhahab, are of epithermal character (Huckerby et al., 1982; Doebrich et al., 1999). The possibility of the presence of porphyry Au–Cu deposits and related skarns and epithermal systems in the Nubian Shield was introduced in several studies (e.g., Ivanov and Hussein, 1972; Hussein, 1990). Hilmy and Osman (1989) described remobilization of gold from a chalcopyrite-pyrite assemblage in the Hamash Au–Cu deposit (SE Egypt), for which Helmy and Kaindl (1999) suggested formation conditions transitional between granitoid-related porphyry style and epithermal vein-type mineralization. Zoheir et al. (2008) described similar conditions of formation for the Semna gold deposit, central Eastern Desert of Egypt, and suggested a genetic link between Au–Cu mineralization and Dokhan Volcanics.

8. Conclusions

Gold mineralization at Wadi Abu Khushayba is related to a NNW–trending auriferous shear zone, in which the ore shoots consist mainly of brecciated quartz and hydrothermally altered, brecciated wallrock and vein fragments. The ore mineralogy is simple, including pyrite and chalcopyrite. Gold is of supergene origin, and is likely to have been liberated by alteration of auriferous sulfides. The absence of replacement textures is suggestive of a single stage of mineralization. The mineralized shear zone is not located on the major NW–SE

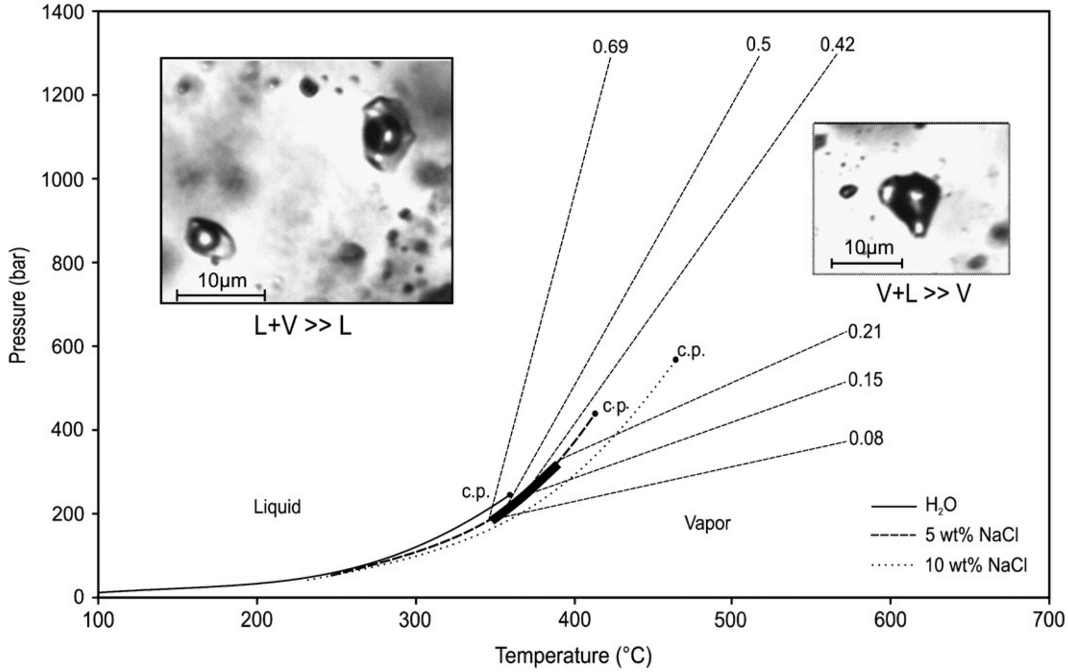

Fig. 9. Intersection of isochores for the vapor-rich and liquid-rich inclusions with the boiling curve (H_2O–NaCl with salinity of 5 wt.% NaCl equiv.) in pressure–temperature space. The isochores are calculated using the equation of state after Zhang and Frantz (1987). The boiling curves of H_2O–NaCl fluids with 0, 5 and 10 wt.% NaCl equiv. and critical points are after Bodnar and Vityk (1994). Insets show coexisting liquid- and vapor-rich inclusions. The thick curve segment represents the proposed *P–T* conditions of the Abu Khushayba gold mineralization.

regional fault system, but is situated on a subsidiary oblique splay fault, typical of structural-controlled vein-type gold deposits. The ore fluids are interpreted to have been focused by differential strain in and around the granophyre bands as a result of the rheological competency contrast between granophyre and volcanic rocks.

The Abu Khushayba gold mineralization shares some characteristics with classical shear-zone related mesothermal or orogenic Au deposits, particularly the non-banded low-sulfide nature of the quartz lodes and the gold-only composition of the veins and mineralized zones. Furthermore, the mineralization style and associated white mica–calcite–albite–quartz alteration assemblage are typical of the orogenic lode-style gold deposits. However, the gold mineralization studied has vein quartz, in which cockade and comb quartz and CO_2-free aqueous fluid inclusions are abundant. The coexistence of vapor- and liquid-rich inclusions, and occurrence of rhombic adularia and calcite point towards boiling as a depositional mechanism, diagnostic for the epithermal environment.

Considering the structural and spatial association of gold with the brecciated rocks and silicic alteration, as well as the fluid inclusion data presented here, we conclude that the Abu Khushayba gold mineralization formed from structurally focused hydrothermal fluids under epithermal conditions (350–380 °C, 200–250 bars). The depth-temperature estimate of the Abu Khushayba mineralization implies a high geothermal gradient (connected to shallow volcanism?) and may reflect a mesothermal–epithermal vein continuum, which is telescoped into the upper 2 to 5 km of continental crust with concomitant igneous activity.

It is possible that the Wadi Abu Khushayba system represents the near surface 'epithermal' expression (epizonal) in a crustal continuum with a deeper orogenic lode system more common in the Arabian–Nubian Shield (cf. Groves et al., 1998).

Acknowledgements

We are grateful to U. Hemmerling and K. Herrmann (TU Clausthal) for the help in sample preparation and electron microprobe analysis, respectively. The manuscript benefited from critical reading by Prof. Hassan Helmy (Minia Univ., Egypt). Reviews by Dr. Nigel Cook (the Editor) and two anonymous referees substantially improved the manuscript and are highly appreciated.

References

Abu Laila, H., Al-Saudi, A., 2002. Geochemical prospecting for gold in Wadi Abu Kusheiba (1996–2001). Hashemite Kingdom of Jordan, National Resources Authority, National Mapping Division, Bulletin.

Akaad, M.K., Noweir, A.M., 1969. Lithostratigraphy of the Hammamat-Um Seleimat district, Eastern Desert, Egypt. Nature 223, 284–285.

Almond, D.C., Ahmed, F., Shaddad, M.Z., 1984. Setting of gold mineralization in the northern Red Sea hills of Sudan. Economic Geology 79, 389–392.

Bakheit, A.K., 1991. Geochemical and tectonic control of sulphide-gold mineralization in Ariab Mineral District, Red Sea Hills, Sudan. Unpublished PhD dissertation, Technical University Berlin, 157 pp.

Bakker, R.J., 2003. Package FLUIDS 1. New computer programs for the analysis of fluid inclusion data and for modelling bulk fluid properties. Chemical Geology 194, 3–23.

Barjous, M., 1992. Geology of the Ash-Shawbak area. Map Sheet 3151 III. Amman, Hashemite Kingdom of Jordan, National Resources Authority, National Mapping Division, Bulletin. 19 pp.

Barjous, M., Mikbel, S., 1990. Tectonic evolution of the Gulf of Aqaba-Dead Sea Transform Fault System. Tectonophysics 180, 49–59.

Baubron, J.C., Delfour, J., Vialette, Y., 1976. Geochronological measurements (Rb/Sr, K/Ar) on rocks of Saudi Arabia. BRGM open-file report 76-JED-22.

Bender, F., 1974. Explanatory notes on the geological map of the Wadi Araba, Jordan: Scale 1:100,000; 3 sheets. Geologisches Jahrbuch B 10, 1–62.

Béziat, P., Bache, J.J., Tawfiq, M.A., Cottard, F., Abdulhay, G., Felenc, J., Bokhari, M., Al-Attas, A., Caïa, J., 1995. Metallic mineral deposits map of the Arabian Shield, Kingdom of Saudi Arabia (Scale 1:1,000,000). DMMR-BRGM joint publication, Jiddah-Orléans, two sheets.

Bielski, M., 1982. Stages in the evolution of the Arabian-Nubian Massif in Sinai. Unpublished Ph.D. Thesis, Hebrew University, Jerusalem, 155 pp.

Bodnar, R.J., 1993. Revised equation and table for determining the freezing point depression of H_2O–NaCl solutions. Geochimica et Cosmochimica Acta 57, 683–684.

Bodnar, R.J., Vityk, M.A., 1994. Interpretation of microthermometric data for NaCl–H2O fluid inclusions. In: De Vivo, B., Frezzotti, M.L. (Eds.), Fluid Inclusions in Minerals: Methods and Applications. Short Course of the Working Group (IMA) “Inclusions in Minerals”, Virginia Polytechnic Institute and State University, Blacksburg, Virginia, pp. 117–131.

Bodnar, R.J., Reynolds, T.J., Kuehn, C.A., 1985. Fluid-inclusion systematics in epithermal systems. Reviews in Economic Geology 2, 73–97.

Brook, M., Ibrahim, K.M., 1987. Geochronological and isotope geological investigation of the Aqaba basement complex of southern Jordan. Unpublished Report, British Geological Survey, Isotope Geology Unit, 48 pp.

Bullen, W., Nimry, F., Okour, M., Abu Laila, H., Al-Saudi, A., 1996. Primary and secondary gold mineralization in Wadi Abu Khushayba, southern Jordan. Natural Resources Authority and Rand Gold Exploration Ltd., South Africa.

Dixon, T.H., Golombek, M.P., 1988. Precambrian crustal accretion rates in northeast Africa and Arabia. Geology 16, 991–994.

Doebrich, J.L., Al-Tayyar, J., Siddiqui, A.A., Al-Otaibi, R., Basahel, M., Zamzami, A., Tarabulsi, Y., 1999. Evaluation of the Ad Duwayhi gold prospect-exploration and characterization of a Neoproterozoic porphyry gold system. Saudi Arabian Deputy Ministry for Mineral Resources Technical Report USGS-TR-99-3. 73 pp.

Doebrich, J.L., Zahony, S.G., Leavitt, J.D., Portacio Jr., J.S., Siddiqui, A.A., Wooden, J.L., Fleck, R.J., Stein, H.J., 2004. Ad Duwayhi, Saudi Arabia: geology and geochronology of a Neoproterozoic intrusion-related gold system in the Arabian Shield. Economic Geology 99, 713–741.

Dubessy, J., 1994. Single components systems: Phase diagrams and their application to fluid inclusions. In: De Vivo, B., Frezzotti, M.L. (Eds.), Fluid Inclusions in Minerals: Methods and applications. Short Course of the Working Group (IMA) “Inclusions in Minerals”, Virginia Polytechnic Institute and State University, Blacksburg, Virginia, pp. 95–115.

El Ramly, M.F., Ivanov, S.S., Kochin, G.C., 1970. The occurrence of gold in the Eastern Desert of Egypt. Studies on some mineral deposits of Egypt. Part I, Section A, Metallic minerals. Annals of the Geological Survey of Egypt 21, 1–22.

Fleck, R.J., Greenwood, W.R., Hadley, D.G., Andersen, R.E., Schmidt, D.L., 1980. Age and evolution of the southern part of the Arabian Shield. Bulletin of the Institute of Applied Geology (Jeddah) 3, 1–17.

Gabra, Sh. Z., 1986. Gold in Egypt: a commodity package. Geological Survey of Egypt, 86 pp, 11 figs and 8 maps.

Garfunkel, Z., 1981. Internal structure of the Dead Sea leaky transform (rift) in relation to plate kinematics. Tectonophysics 80, 81–108.

Garson, M.S., Shalaby, I., 1976. Precambrian-lower Palaeozoic plate tectonics and metallogenesis in the Red Sea region. Geological Association of Canada, Special Paper 14, 573–596.

Greenwood, W., Hadly, D., Anderson, R., Fleck, R., Schmidt, D., 1976. Late Proterozoic cratonisation in the southwest of Saudi Arabia. Philosophical Transactions, Royal Society of London A280, 517–527.

Groves, D.I., Goldfarb, R.J., Gebre-Mariam, M., Hagemann, S.G., Robert, F., 1998. Orogenic gold deposits: a proposed classification in the context of their crustal distribution and relationship to other gold deposit types. Ore Geology Reviews 13, 7–27.

Hargrove, U.S., Stern, R.J., Kimura, J.I., Manton, W.I., Johnson, P., 2006. How juvenile is the Arabian–Nubian Shield? Evidence from Nd isotopes and pre-Neoproterozoic inherited zircons. Earth and Planetary Science Letters 252, 308–326.

Harraz, H.Z., 2000. A genetic model for a mesothermal Au deposit: evidence from fluid inclusions and stable isotopic studies at El-Sid Gold Mine, Eastern Desert. Journal of African Earth Science 30, 267–282.

Hauptmann, A., 2007. The Archaeometallurgy of Copper: Evidence from Faynan, Jordan. Springer, Berlin. 388 pp.

Helmy, H.M., Kaindl, R., 1999. Mineralogy and fluid inclusion studies of the Au–Cu quartz veins in the Hamash area, South-Eastern Desert, Egypt. Mineralogy and Petrology 65 (1–2), 69–86.

Helmy, H.M., Kaindl, R., Fritz, H., Loizenbauer, J., 2004. The Sukari gold mine, Eastern Desert-Egypt: structural setting, mineralogy and fluid inclusion study. Mineralium Deposita 39, 495–511.

Hilmy, M.E., Osman, A., 1989. Remobilization of gold from a chalcopyrite-pyrite mineralization: Hamash gold mine, Southeastern Desert, Egypt. Mineralium Deposita 24, 244–249.

Huckerby, J.A., Moore, J.MacM., Davis, G..R., 1982. Mineralization and structure at the Mahd Adh Dhahab Gold mine, Saudi Arabia. Abstract in Precambrian Research A2 416 pp.

Hussein, A.A., 1990. Mineral deposits. In: Said, R. (Ed.), The Geology of Egypt. Balkema, Rotterdam, pp. 511–566.

Ibrahim, K.M., McCourt, W.J., 1995. Neoproterozoic granitic magmatism and tectonic evolution of the northern Arabian Shield: evidence from Southwest Jordan. Journal of African Earth Science 20, 103–118.

Ivanov, T., Hussein, A.A., 1972. On geological operations carried out from July, 1968 to June, 1972. In: Assessment of the mineral potential of the Aswan region, United Nations Development Program, Technical Report, Cairo (unpublished report).

Jarrar, G., Baumann, A., Wachendorf, H., 1983. Age determinations in the Precambrian basements of the Wadi Araba area, southwest Jordan. Earth and Planetary Science Letters 63, 292–304.

Jarrar, G., Wachendorf, H., Zellmer, H., 1991. The Saramuj conglomerate: evolution of a Pan-African molasse sequence from southwest Jordan. Neues Jahrbuch für Mineralogie und Palaeontogie 335–356.

Jarrar, G., Wachendorf, H., Zachmann, D., 1993. A Pan-African pluton intruding the Saramuj Conglomerate, south-west Jordan. Geologische Rundschau 82, 121–135.

Johnson, P.R., Abdelsalam, M.G., Stern, R.J., 2003. The Bi'r Umq-Nakasib Suture Zone in the ANS: a key to understanding crustal growth in the East African Orogen. Gondwana Research 6, 523–530.

Kusky, T.M., Ramadan, T.M., 2002. Structural controls on Neoproterozoic mineralization in the South Eastern Desert, Egypt: an integrated field, Landsat TM, and SIR-C/X SAR approach. Journal of African Earth Sciences 35, 107–121.

LeAnderson, P.J., Yoldash, M., Johnson, P.R., Offield, T.W., 1995. Structure, vein paragenesis, and alteration in the Al Wajh gold district, Saudi Arabia. Economic Geology 90, 2262–2273.

Lenz, H., Bender, F., Besang, C., Harre, W., Kreuzer, H., Müller, P., Wendt, I., 1972. The age of the early tectonic events in the zone of Jordan geosuture based on radiometric data. Proceedings of the 24th International Geological Congress, Section 3, pp. 371–379.

Loizenbauer, J., Neumayr, P., 1996. Structural controls on the formation of the Fawakhir gold mine, El Sid-Eastern Desert, Egypt: tectonic and fluid inclusion evidence. Proceedings of the Centennial Conference of the Geological Survey of Egypt, pp. 477–488.

McCourt, W.J., 1988. The geology, geochemistry and tectonic setting of the granitic rocks of SW Jordan. Hashemite Kingdom of Jordan. Natural Resource Authority, Geology Directorate, Bulletin of the Geological Mapping Division, 10.

Moghazi, A.M., 2003. Geochemistry and petrogenesis of a high-K calc–alkaline Dokhan Volcanic Suite, South Safaga area, Egypt: the role of late Neoproterozoic crustal extension. Precambrian Research 125, 161–178.

Pearce, J.A., Harris, N.B.W., Tindle, A.G., 1984. Trace element discrimination diagrams for the tectonic interpretation of granitic rocks. Journal of Petrology 25, 956–983.

Pohl, W., 1988. Precambrian metallogeny of NE-Africa. In: El-Gaby, S., Greiling, R.O. (Eds.), The Pan-African Belt of NE Africa and adjacent areas. Friedrich Vieweg und Sohn, Braunschweig-Wiesbaden, pp. 319–341.

Rabba, I., 1994. Geology of the Qurayqira (Jabal Hamra Fadan). Map Sheet 3051 II. Amman, Hashemite Kingdom of Jordan. Natural Resource Authority, Geology Directorate, Bulletin of the Geological Mapping Division. 28 pp.

Rabba, I., Ibrahim, K.M., 1988. Petrography of the plutonic rocks of the Aqaba Complex, Jordan. Hashemite Kingdom of Jordan. Natural Resource Authority, Geology Directorate: Bulletin of the Geological Mapping Division, 9. 86 pp.

Rabba, I., Masri, A., Moumani, K., Gharaibeh, A., Khraisat, K., 1999. Geological Map of Wadi Abu Khushayba, 1:10,000 (Gold Exploration Project). Hashemite Kingdom of Jordan. Natural Resource Authority, Geology Directorate, Bulletin of the Geological Mapping Division. 12 pp.

Rashdan, M., 1988. The geology of Aqaba and Wadi Araba area, Map Sheets No. 3049-III; 2949-II, Hashemite Kingdom of Jordan. Natural Resource Authority, Geology Directorate, Bulletin of the Geological Mapping Division 7 87 pp.

Roedder, E., Bodnar, R.J., 1980. Geologic pressure determinations from fluid inclusions studies. Annual Review of Earth and Planetary Sciences 8, 263–301.

Sabet, A.H., Bondonosov, V.P., 1984. The gold ore formations in the Eastern Desert of Egypt. Annals of the Geological Survey of Egypt 14, 35–42.

Sabir, H., 1991. Ancient mining and its impact on modern mineral exploration in Saudi Arabia. Saudi Arabian Directorate General of Mineral Resources Technical Report BRGM-TR-11-3. 31 pp.

Shepherd, T.J., Rankin, A.H., Alderton, D.H.M., 1985. A Practical Guide to Fluid Inclusion Studies. Blackie, Glasgow. 239 pp.

Stern, R.J., Hedge, C.E., 1985. Geochronologic and isotopic constraints on Late Precambrian crustal evolution in the Eastern Desert of Egypt. American Journal of Science 285, 97–127.

Sylvester, P.J., 1989. Post-collisional alkaline granites. Journal of Geology 97, 261–280.

Taylor, S.R., McLennan, S.M., 1995. The geochemical evolution of the continental crust. Reviews of Geophysics 33, 241–265.

Tolessa, D., Pohl, W., 1999. Constraints on interpretation of geochemical data for gold exploration in multiply deformed and metamorphosed areas: an example from Lega Dembi gold deposit, southern Ethiopia. Journal of African Earth Sciences 29, 367–380.

Vail, J.R., 1987. Late Proterozoic tectonic terranes in the Arabian–Nubian Shield and their characteristic mineralization. Geological Journal 22, 161–174 (thematic issue).

Winchester, J.A., Floyd, P.A., 1977. Geochemical discrimination of different magma series and their differentiation products using immobile elements. Chemical Geology 20, 325–343.

Zhang, Y., Frantz, J.D., 1987. Determination of the homogenization temperatures and densities of supercritical fluids in the system NaCl–KCl–$CaCl_2$–H_2O using synthetic fluid inclusions. Chemical Geology 64, 335–350.

Zoheir, B.A., 2008. Structural controls, temperature–pressure conditions and fluid evolution of orogenic gold mineralisation in Egypt: a case study from the Betam gold mine, south Eastern Desert. Mineralium Deposita 43, 79–95.

Zoheir, B.A., Akawy, A., Hassan, I., 2008. Role of fluid mixing and wallrock sulfidation in gold mineralization at the Semna mine area, central Eastern Desert of Egypt: evidence from hydrothermal alteration, fluid inclusions and stable isotope data. Ore Geology Reviews 34, 580–596.